

Article

Electrochemical Detection of Dopamine: Novel Thin-Film Ti-Nanocolumnar Arrays/Graphene Monolayer-Cu_{foil} Electrodes

Georgia Balkourani ¹, José Miguel García-Martín ², Elena Gorbova ^{1,3}, Carmelo Lo Vecchio ⁴, Vincenzo Baglio ⁴, Angeliki Brouzgou ^{5,*} and Panagiotis Tsiakaras ^{1,3,*}

¹ Laboratory of Alternative Energy Conversion Systems, Department of Mechanical Engineering, School of Engineering, University of Thessaly, Pedion Areos, 38834 Volos, Greece; gbalkourani@gmail.com (G.B.); e.gorbova@ihite.ru (E.G.)

² Instituto de Micro y Nanotecnología (IMN-CNM), CSIC (CEI UAM+CSIC), Isaac Newton 8, Tres Cantos, 28760 Madrid, Spain; josemiguel.garcia.martin@csic.es

³ Laboratory of Electrochemical Devices Based on Solid Oxide Proton Electrolytes, Institute of High Temperature Electrochemistry (RAS), Yekaterinburg 620990, Russia

⁴ Institute of Advanced Energy Technologies “Nicola Giordano”, Consiglio Nazionale delle Ricerche, Via Salita Santa Lucia sopra Contesse, 5, 98126 Messina, Italy; lovecchio@itae.cnr.it (C.L.V.); vincenzo.baglio@itae.cnr.it (V.B.)

⁵ Department of Energy Systems, School of Technology, University of Thessaly, Geopolis, Regional Road Trikala-Larisa, 41500 Larisa, Greece

* Correspondence: amprouzgou@uth.gr (A.B.); tsiak@uth.gr (P.T.)

Abstract: Deposition at oblique vapor incidence angles can lead to the growth of thin films with dramatically changed morphological features. Herein, thin-film titanium nanocolumnar arrays were grown on a graphene monolayer/copper foil substrate (Ti_{NCs}/G_m-Cu_{foil}) by applying a physical vapor deposition method, through magnetron sputtering at an oblique angle. Ti-nanocolumnar arrays with ca. 200 nm length were developed throughout the substrate with different morphologies depending on the substrate topography. It was found that over the as-fabricated electrocatalyst, the electrooxidation reaction of dopamine is facilitated, allowing quasi-reversible electrooxidation of protonated dopamine to dopamine quinone. Additionally, contrary to works that appeared in the literature, Ti_{NCs}/G_m-Cu_{foil} also promotes further quasi-reversible oxidation of leucodopaminechrome to dopaminochrome. The electrode exhibited two linear ranges of dopamine detection (10–90 μM with a sensitivity value of 0.14 μAμM⁻¹cm⁻² and 100–400 μM with a sensitivity value of 0.095 μAμM⁻¹cm⁻²), a good stability over time of about 30 days, and a good selectivity for dopamine detection.

Keywords: dopamine electrochemical sensor; thin-film electrode; titanium nanocolumnar arrays; graphene monolayer; magnetron sputtering; oblique angle deposition



Citation: Balkourani, G.; García-Martín, J.M.; Gorbova, E.; Lo Vecchio, C.; Baglio, V.; Brouzgou, A.; Tsiakaras, P. Electrochemical Detection of Dopamine: Novel Thin-Film Ti-Nanocolumnar Arrays/Graphene Monolayer-Cu_{foil} Electrodes. *Catalysts* **2024**, *14*, 478. <https://doi.org/10.3390/catal14080478>

Academic Editor: Nicolas Alonso-Vante

Received: 1 July 2024

Revised: 23 July 2024

Accepted: 25 July 2024

Published: 27 July 2024



Copyright: © 2024 by the authors. Licensee MDPI, Basel, Switzerland. This article is an open access article distributed under the terms and conditions of the Creative Commons Attribution (CC BY) license (<https://creativecommons.org/licenses/by/4.0/>).

1. Introduction

Neurotransmitters are chemical substances that transfer chemical messages between the brain cells. Dopamine (DA) is a nitrogen-containing organic compound and a vital neurotransmitter that regulates multiple functions of the mammalian hormonal, circulatory, and central nervous systems, playing key functions in human health and cognition [1]. Disturbances in dopamine levels are linked to neurological diseases; for instance, Parkinson's, Alzheimer's, depression, and more [1]. Therefore, achieving accurate, real-time, and efficient detection of dopamine levels in the human body is vital.

Noble metal electrocatalysts have been extensively studied for electrochemical oxidation [2,3], and sensing applications at high [4–6] and low temperature [7–9], including neurotransmitter detection. Although noble metals exhibit great performance in detecting biomolecules, they are expensive and present restricted selectivity. Thus, non-enzymatic

detection employing non-noble metal nanoparticles and carbonaceous substances as electrocatalysts is currently dominating the research field of biomolecule electrochemical sensing [10,11].

Graphene is one of the most attractive carbon nanomaterials with a 2D honeycomb-like hexagonal lattice composed of sp^2 -hybridized carbons [12]. Due to its structure, graphene has one of the larger surface areas to volume ratios among novel 2D crystalline-layered materials and possesses also excellent electrical conductivity. However, the conductivity of graphene decreases with increasing thickness (number of layers from 2–13) [13]. Compared with the few-layer graphene, a graphene monolayer exhibits better properties in many technological applications due to its high crystallinity and the lack of layers stacking. It has been shown experimentally that the mechanical properties of graphene are more sensitive to temperature changes when the number of layers increases [14].

Graphene can be grown or deposited on metallic surfaces with different methods. Chemical vapor deposition has proven to be one of the most promising methods for depositing monolayer graphene on metallic substrates [15]. The primary use of graphene grown on thin-metal films is electrochemical device fabrication, in which conductivity and electron and hole mobility are critical. As reported in the literature [16], a multilayer “thick” graphene is formed when nickel is the chosen substrate, while a monolayer “thin” graphene is obtained when copper is the substrate of choice. Therefore, copper substrates, such as copper foil, are used to grow a single and bi-layer graphene. Electrochemical biomolecule detection sensors demand substrates with great electrical conductivity [17]. Transition metals as substrate materials exhibit suitable properties for electrochemical applications, such as the ability to form stable complexes, often with profound catalytic activity. Thus, copper foil seems an ideal choice as a substrate mainly due to its high electrical conductivity and low cost [18].

In the last few years, titanium and its alloys have been among the most widely explored and promising materials concerning medical applications [19,20]. In their recent review study, García-Martín et al. [21] highlighted the extended use of TiO_2 in electrochemical sensing applications due to its electrocatalytic activity. The authors also concluded that Ti can form coordination bonds with the carboxyl and amino groups. As the DA molecule has an amino group, it is possible to be selectively detected from Ti-electrocatalysts. Titanium, despite its proven biocompatibility [22], has not been explored as a basic electrode material for dopamine electrochemical sensors, as much as might have been expected. The thickness of the working electrode (i.e., the catalytic layer thickness) as a key factor for the sensor performance should be methodically studied. Too thin electrodes may lead to the sensor collapse, while too thick increases the sensor resistance.

Wang et al. [23] explored DA electrochemical detection over a carbon-titanium nitride-modified glassy carbon electrode (C-TiN/GCE). The as-fabricated electrode achieved a great limit of detection and excellent sensitivity. The DA electrooxidation was probably catalyzed synergistically by the carbon and titanium nitride, which enhanced interfacial electron transfer. Feng et al. [24] modified a glassy carbon electrode (GCE) with a nanocomposite of titanium nitride (TiN) on reduced graphene oxide (rGO) (TiN-rGO/GCE). The as-prepared electrode was employed for the co-detection of DA and uric acid in the presence and absence of ascorbic acid. TiN-rGO/GCE showed a wide linear detection range for both dopamine (DA) and uric acid (UA). The good selectivity and sensitivity against DA were attributed to the formation of positive charges on the electrode and hence the electrostatic attractions between the DA molecules and electrode surface. Recently, Paul et al. [25] prepared a nanocomposite of metal-organic-framework (MOF) and titanium carbide (Ti_3C_2) for DA electrochemical detection. The MOF's crystalline structure offered electrostatic and π - π interactions between the DA and the pyromellitic acid, while Ti_3C_2 performed as the charge transporter, giving and receiving electrons.

Titanium and its alloys present high biocompatibility, which enables their usage in (bio)medical applications. As recently shown [26–28], different morphologies of Ti change

the surface free energy, thus permitting the determination of the optimal surface topography for each application.

Taking advantage of previous works [29,30] in combination with the importance of surface chemistry [31] in the performance of electrochemical sensors led us to the fabrication of nanostructured thin films made of titanium nanocolumns which were grown by oblique angle deposition with magnetron sputtering on a graphene monolayer Cu foil substrate ($\text{Ti}_{\text{NCs}}/\text{G}_m\text{-Cu}_{\text{foil}}$). The development of the Ti-nanocolumnar film is the outcome of the atomic shadowing mechanism and diffusion processes associated with the quite high kinetic energy of the sputtered atoms [29]. To our knowledge, similar electrodes have not yet been examined in international literature. The adopted substrate is expected to impart to our electrode the expected interfacial electron transfer ability.

2. Results and Discussion

2.1. Morphology and Surface Characterization

The surface of the substrate exhibits two different morphologies: regions with ridges (the most frequent scenario) and some flat regions (Figure S1a). The AFM characterization (Figure S1b) reveals the variety in the morphology of the substrate. This variety had consequences on the morphology of the titanium nanocolumnar film growth which is also easily discernible by eye (Figure S1c,d). SEM images, Figure 1a,b, show the different morphologies of the substrate, indicating flat areas and areas of ridges. This difference might be ascribed to the Cu material topography making graphene wrinkle up in some areas (Figure 1b).

Figure 1c,d shows top-view SEM micrographs of Ti nanopillars formed on the ridges of the $\text{G}_m\text{-Cu}_{\text{foil}}$ substrate parallel to the atomic flux during deposition and of those grown in a region of the substrate with ridges nearly perpendicular to the atomic flux, respectively. Moreover, some small areas with grown Ti nanocolumns on flat substrate areas were also observed (Figure 1e). The atomic flux direction during Ti deposition is indicated with a white arrow in Figure 1c.

The SEM observations are confirmed by the AFM results according to which the average height of the nanopillars is ca. 200 nm. As can be seen in Figure 2a,b, when the ridges of the substrate are almost aligned with the direction of the atomic flux during the deposition of Ti, a well-distributed and homogeneous Ti-nanocolumnar array is developed, quite similar to arrays obtained on flat Si substrates [29].

However, in the regions where the substrate ridges are nearly vertical to the direction of the incoming atomic flux, the Ti nanocolumns form only at the tallest features (for example, at the edges of the ridges), as illustrated in Figure 2c,d, because the step structure of the ridges causes shadowing effects that prevent the formation of nanocolumns [10]. The atomic flux direction during Ti deposition is indicated with a white arrow in Figure 2a,c.

The electrode composition is given in Table 1. Cu is at the highest concentration (66.7 at. %), then C is the second element in abundance (15.6 at. %), and the Ti atomic percentage was found to be 6.3 at. %. N, O, and part of the C can be ascribed to the exposure of the electrode at ambient conditions. In fact, in previous work [32], it was shown that crystalline TiO_2 rutile was formed on the first outer atomic monolayers of the columns, but such a layer did not significantly affect the performance of the Ti nanocolumns as bioelectrodes in PBS [30].

Generally, Ti nanocolumns have been grown throughout the substrate, with different morphologies and distributions depending on the characteristics of each substrate area. As illustrated in Figure 3, depending on the orientation of the steps to the atomic flux during the deposition, a shadow can be created, that might prevent the formation of nanocolumns or can have a negligible effect. That depends on whether the ridges are perpendicular or parallel to the in-plane projection of the atomic flux, respectively.

Table 1. Elemental analysis of the $\text{Ti}_{\text{NCs}}/\text{G}_m\text{-Cu}_{\text{foil}}$.

Element	Weight %	Atomic %
C	3.8	15.6
N	2.8	9.7
O	0.3	1.7
Ti	6.2	6.3
Cu	86.9	66.7

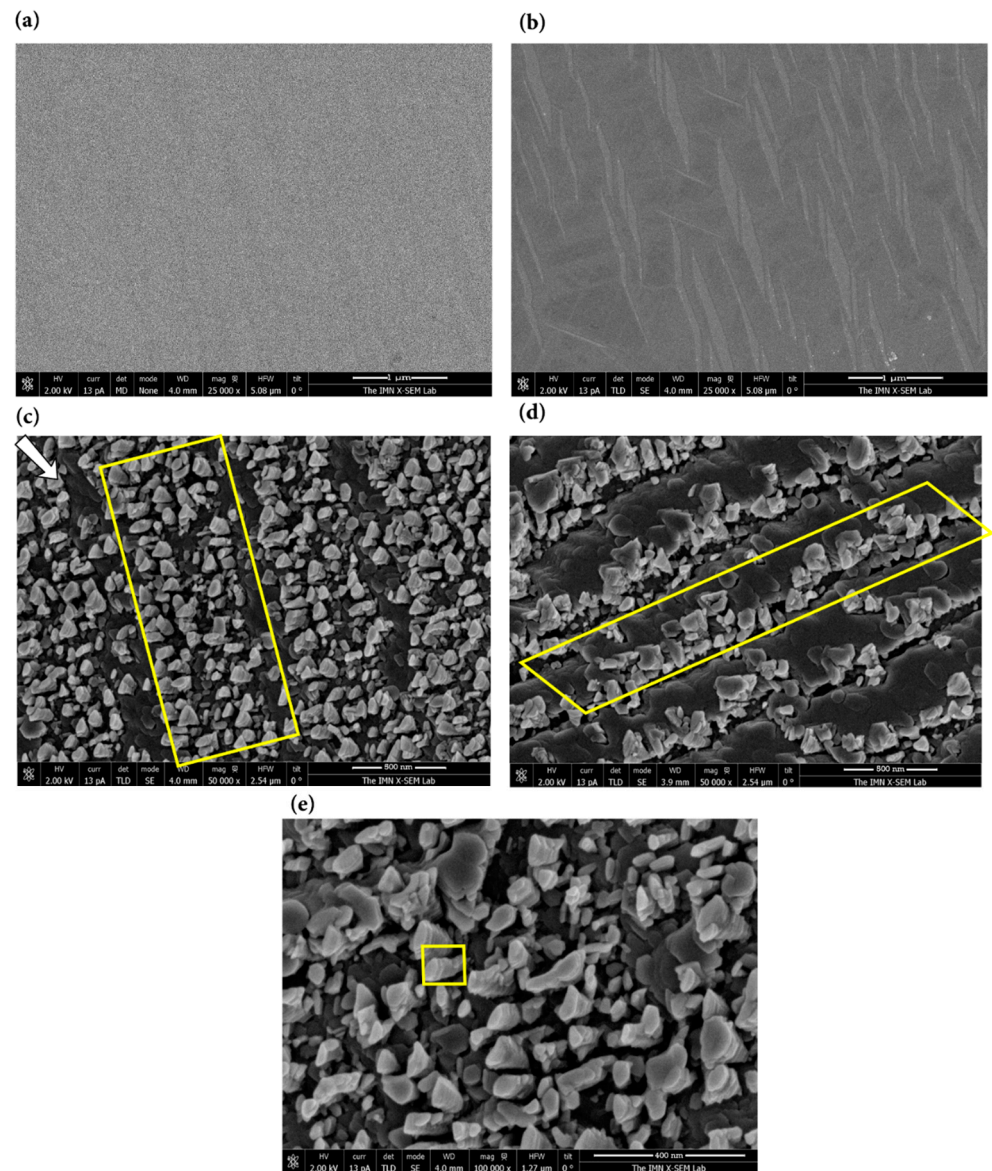


Figure 1. SEM images of the $\text{G}_m\text{-Cu}_{\text{foil}}$ flat region (a) and the $\text{G}_m\text{-Cu}_{\text{foil}}$ region with ridges (b), SEM images of the Ti nanocolumns grown on different regions of the $\text{G}_m\text{-Cu}_{\text{foil}}$ substrate: nanocolumns grown in a region with ridges that were parallel to the atomic flux during the deposition (c), in a region with ridges that were almost perpendicular to such atomic flux (d) and in a region that was initially almost flat (e), respectively.

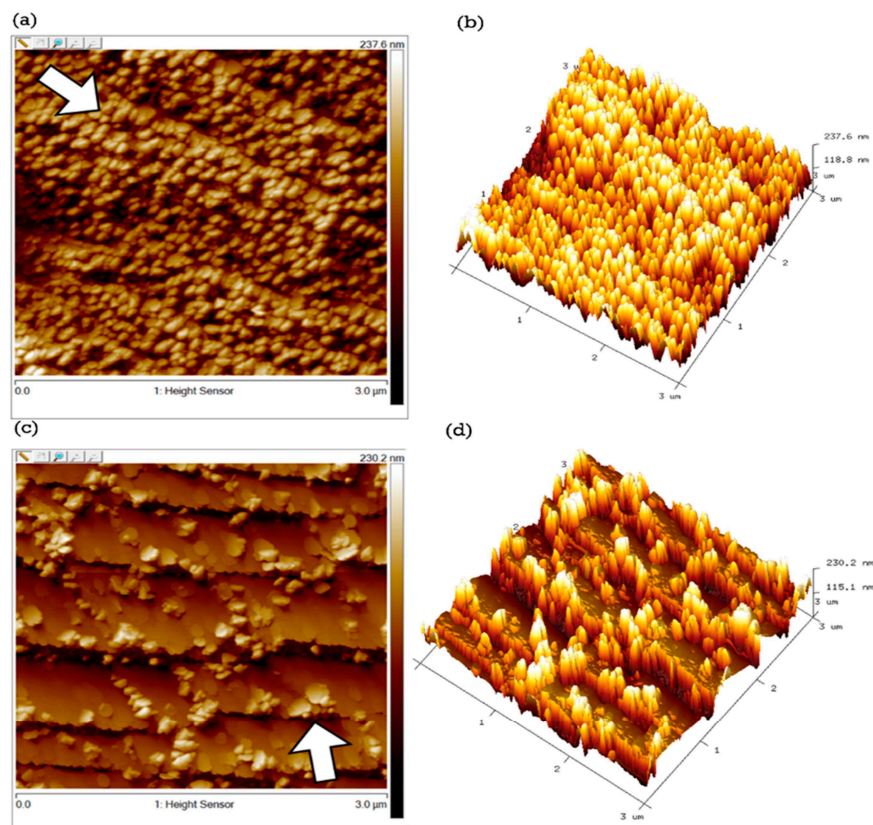


Figure 2. Representative AFM images of different regions of the electrode (a,c) show standard 2D images, whilst (b,d) show 3D representations of the same data, respectively.

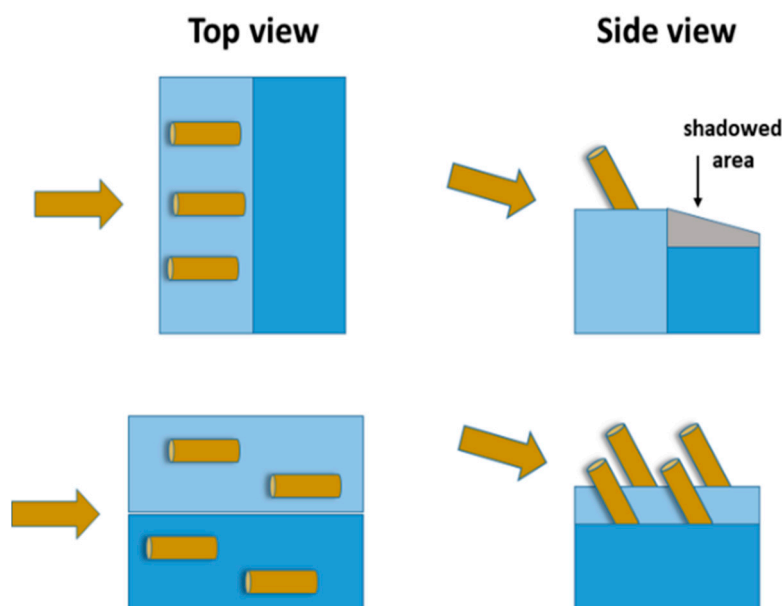


Figure 3. Top view and side view of the Ti nanocolumns growth depending on the orientation of the steps concerning the atomic flux during the deposition.

2.2. Electrochemical Performance of the Ti_{NCs}/G_m-Cu_{foil}

The dopamine (DA) electrochemical reaction mechanism was initially investigated on the surface of the Ti_{NCs}/G_m-Cu_{foil} electrode with CV measurements at various scan rates. Then, using the DPV technique, the electrochemical detection characteristics of the as-fabricated electrode for the dopamine molecule were evaluated. Additionally, the

long-term stability, storage ability, and selectivity of the electrode were estimated, using the CA technique.

2.2.1. Dopamine Electrooxidation Reaction Mechanism

The CV behavior of the as-fabricated electrode in PBS (CV blind) and then in the 0.1 mM dopamine in PBS solution is shown in Figure 4a. All voltages are relative to Ag/AgCl reference electrode. In the case of pure PBS, one well-defined redox pair of peaks appears. The one during the direction of positive scanning is observed at around 0.03 V, and the other during the negative potential scanning, at ca. -0.30 V. According to the literature [33], the observed anodic peak could be assigned to TiO_2 formation, while the cathodic peak might be attributed: (1) to the formation of lower valence states, specifically Ti^{3+} formed in the TiO_2 anodic oxidation film, (2) the titanium hydroxide, and (3) the H^+ adsorbed on the reduction of the oxide, formed previously in the anodic scan.

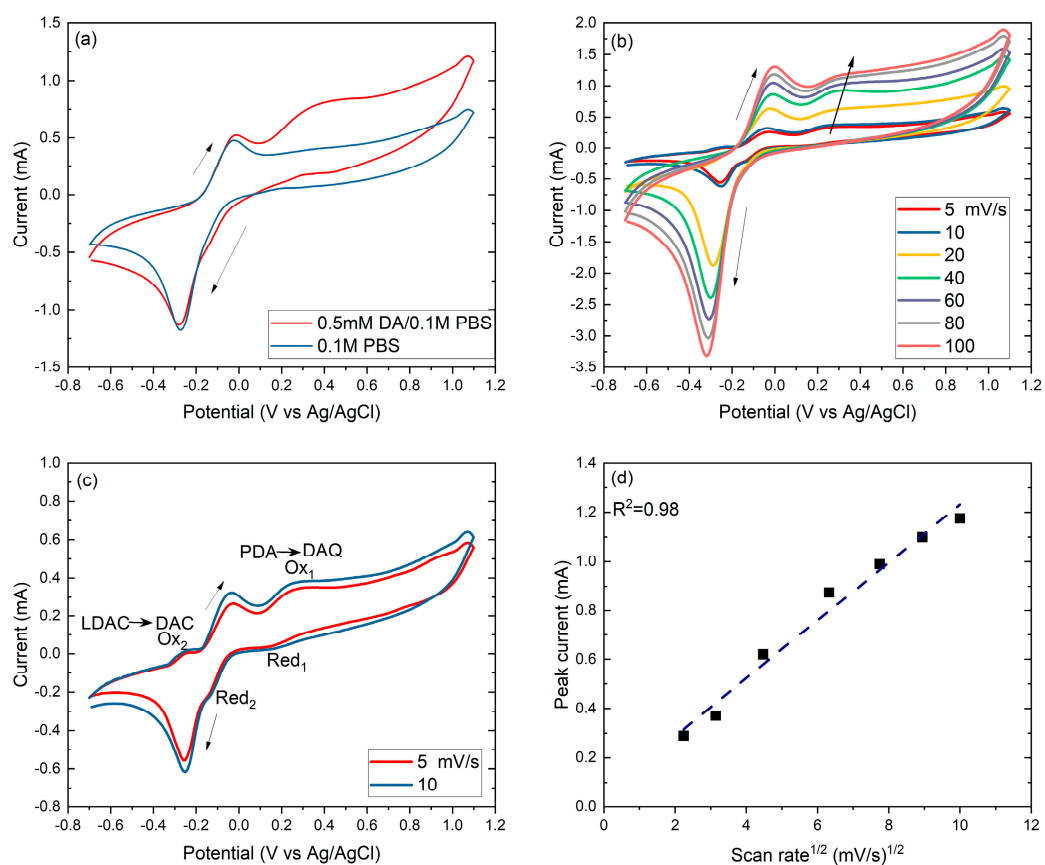


Figure 4. Cyclic voltammograms of the $\text{Ti}_{\text{NCs}}/\text{G}_m\text{-Cu}_{\text{foil}}$ electrode in the absence and presence of 0.5 mM DA, in 0.1 M PBS electrolyte of pH = 7.0, at $T = 36.6$ °C, and 20 mV/s scan rate (a), CV curves of the $\text{Ti}_{\text{NCs}}/\text{G}_m\text{-Cu}_{\text{foil}}$ electrode at different scan rates—in 0.5 mM DA, in 0.1 M PBS electrolyte (b), CVs of the $\text{Ti}_{\text{NCs}}/\text{G}_m\text{-Cu}_{\text{foil}}$ electrode at 5 and 10 mV/s in 0.5 mM DA, in 0.1 M PBS electrolyte (c), Corresponding oxidation peak current (at +0.35 V) vs. square root of scan rate (d).

However, according to Azumi et al. [34], the second option is more likely to occur at potential values above 3 V, while taking into consideration the type of electrolyte used herein which does not contain compounds that can give H^+ , the third option is not very likely. Thus, for the synthesized electrode, the appearance of the cathodic peak is attributed to the first option. The cathodic peak potential depends on the anodic potential threshold. Usually, it appears at around -0.36 V [33], whereas, in this work, it appears at approximately -0.30 V.

In the presence of dopamine (Figure 4a), during the forward scanning, a broad oxidation peak appears with a peak potential at around +0.35 V. According to the

literature [35–39], when the pH value of the dopamine solution falls in the interval between 5.8–7.0, protonated dopamine (PDA) is the predominant species in the diffusion layer.

According to the generally accepted mechanism [35–39], the oxidation peak at +0.35 V could be ascribed to the $2e^-$ transfer due to the electrochemical oxidation reaction of the PDA to dopamine quinone (DAQ) (Figure 4a). However, for further examination of the dopamine oxidation reaction (DOR) mechanism over our electrode, CV measurements at different scan rates were performed, as shown in Figure 4b,c. The CV curves are similar from 20 to 100 mV/s, indicating an oxidation peak (PDA→DAQ) at ca. +0.35 V. The increment of the scan rate results in peak currents increment and shift of peak potentials to more positive values, thus suggesting a diffusion-controlled process. This is validated by Figure 4d, where the anodic peak currents are quite linearly proportional to the square root of the scan rate [40–42].

However, this is not the case for the lower scan rates (Figure 4c). The voltammograms at 5 and 10 mV/s during the forward scanning also present the oxidation peak at ca. +0.35 V (PDA→DAQ) but is followed by a smaller wide reduction peak at ca. +0.17 V, which is associated with DAQ to PDA reduction [21]. The peak separation is $|E_{p,a} - E_{p,c}| = 180$ mV, suggesting a quasi-reversible redox behavior. DAQ must remain adsorbed to the electrode surface to reduce back to dopamine during the backward scanning [40]. However, the reduction peak current is much smaller than the oxidation, indicating that PDA oxidation is quasi-reversible and DAQ desorbs before the cathodic scan. The PDA→DAQ redox reaction is a $2e^-$ transfer, according to which DAQ is formed and is partly reduced back to PDA [35–38]. The second oxidation peak appears at ca. −0.25 V and the reduction peak at ca. −0.14 V, during the backward scanning, yielding a 110 mV peak separation (ΔE_p) (Figure 4c). The lower peak separation of the second redox couple indicates that the affiliated redox reaction is faster than the PDA→DAQ but still retains a quasi-reversible behavior. When amine form is deprotonated, then an autochemical ring closure reaction follows, forming leucodopaminechrome (LDAC) (Figure 5) [35–38].

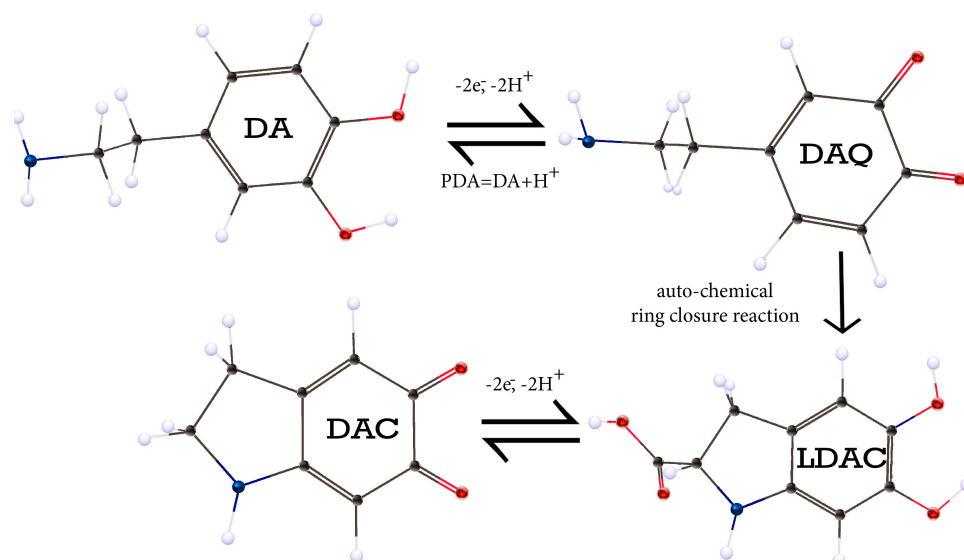


Figure 5. Suggested dopamine electrooxidation mechanism over the $Ti_{1}NCs/G_m-Cu_{foil}$ electrode. A dopamine molecule in the form of protonated dopamine (PDA) is oxidized to dopamine quinone (DAQ), which is auto-converted to leucodopaminechrome (LDAC), which is oxidized to dopaminechrome (DAC).

According to the literature [35], the oxidation peak at −0.25 V is ascribed to LDAC oxidation to dopaminechrome (DAC) (LDAC→DAC), and the reduction peak at −0.14 V to the reduction of DAC back to LDAC. It is generally accepted [35–39] that LDAC is easier to oxidize than PDA, undergoing a $2e^-$ oxidation process that leads to DAC formation.

As the bibliography confirms [43], during anodic oxidation, different types of titanium oxides may be formed on the titanium surface (e.g., TiO, TiO₂, Ti₂O₃, and Ti₃O₅). Among them, TiO₂ is the most stable and frequently found oxide, as observed in the oxidation peak at -0.03 V of the 0.1 M PBS curve, in Figure 4a. Thus, it can be assumed that the PDA to DAQ and the LDAC to DAC anodic oxidations at ca. $+0.35$ V and -0.25 V (Figure 4c) can be catalyzed from the different intermediate oxide formations.

As depicted in Figure 5, the suggested mechanism agrees with the literature [35–37] following the electron transfer-chemical transfer-electron transfer route. In the literature, most materials explored for the dopamine electrooxidation reaction favor the first redox couple [41,44–48], i.e., the electrochemical oxidation reaction of PDA to DAQ.

Over Ti_{NCs}/G_m-Cu_{foil} electrode, dopamine electrooxidation reaction is facilitated, allowing the second redox couple's reaction (LDAC \rightleftharpoons DAC). The electrode's distinctive nanocolumnar arrays being fabricated at $\theta = 75^\circ$ oblique angle could offer a morphology with abundant active sites near the interface. Thin-film Ti nanostructures seem to operate synergistically with the graphene monolayer facilitating charge transfer, thus permitting the LDAC \rightleftharpoons DAC redox reaction.

2.2.2. Dopamine Calibration Curve and Sensitivity

Figure 6a depicts a series of DPV curves recorded at various DA concentrations in 0.1 M (mol L⁻¹) PBS, for the Ti_{NCs}/G_m-Cu_{foil} electrode. A linear increase trend is observed at DA concentrations from 10 μ M to 90 μ M DA, while a second linear range is observed for higher concentrations from 100 μ M to 400 μ M DA (Figure 6b). The respectively obtained regression equations are: I_p (μ A) = $4.97 + 0.14 \times C$ (μ M) with $R^2 = 0.995$, and I_p (μ A) = $11.065 + 0.095 \times C$ (μ M) with $R^2 = 0.987$.

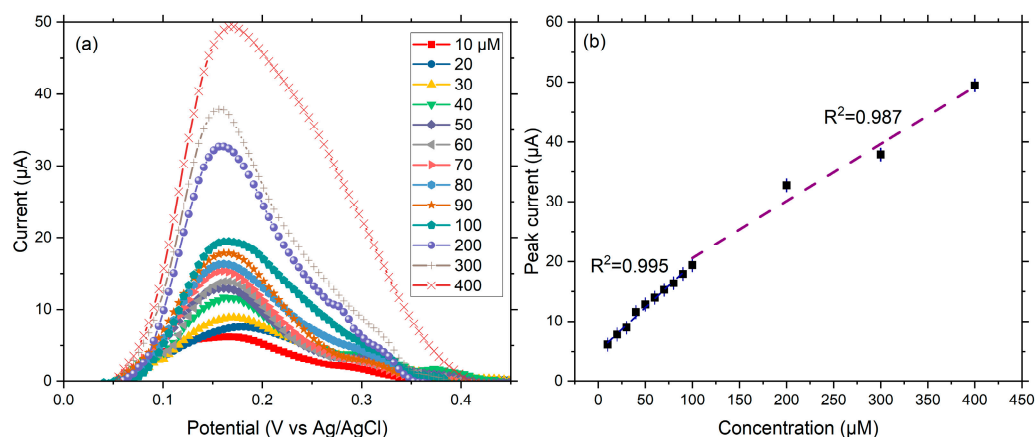


Figure 6. (a) Differential pulse response of the Ti_{NCs}/G_m-Cu_{foil} electrode for different DA concentration values in 0.1 M PBS electrolyte solution, and (b) linear response of the DA oxidation current vs. concentration values (calibration curve).

The sensitivity for the first linear range (10–90 μ M) was calculated at $0.14 \mu\text{A}\mu\text{M}^{-1}\text{cm}^{-2}$, and for the second (100–400 μ M) at $0.095 \mu\text{A}\mu\text{M}^{-1}\text{cm}^{-2}$, using Equation (1) below:

$$\text{Sensitivity} = \frac{S}{A} \quad (1)$$

where $S_1 = 0.14$ ($\mu\text{A}\mu\text{M}^{-1}$) and $S_2 = 0.095$ ($\mu\text{A}\mu\text{M}^{-1}$) are the slopes of the first and the second calibration curve (Figure 6b), respectively, and $A = 1$ (cm^2) is the geometric area of the working electrode.

The limit of detection (LOD) was calculated using the following equation (Equation (2)):

$$\text{LOD} = 3 \times \left(\frac{\sigma}{S} \right) \quad (2)$$

where ~ 3 is the signal-to-noise ratio (S/N) [49,50], $\sigma = 0.31$ is the standard deviation of the y-intercept [51], and $S_1 = 0.14$ is the slope of the lower concentration values, both graphically calculated of the calibration curve.

2.2.3. Selectivity, Long-Term Stability, and Repeatability

Selectivity is also considered a significant parameter for the operation of electrochemical sensors. Some of the most common interfering compounds co-existing with DA in the human body, such as ascorbic acid (AA), uric acid (UA), and glucose (Glu) [52], were chosen to investigate the selectivity of the $\text{Ti}_{\text{NCs}}/\text{G}_m\text{-Cu}_{\text{foil}}$ electrode. The representative amperometric current response, at a potential close to DA's oxidation (0.175 V), upon successive addition of 1 mM DA, Glu, UA, AA, and DA is shown in Figure 7a. The current response reaches an almost stable value after 75 s. Thus, this time interval (75 s) was chosen between the interferences' additions. The DA addition causes an increment of 85% in the current response, while the addition of Glu and UA only slightly alters the current. Here, it should be noted, that a small initial current response originates from the addition/drop of the different interference and does not correspond to an actual current from the interference detection. Later, AA is added, and a weak current response is observed. Then, at the 2nd drop of the DA, the respective current is much higher from its 1st drop. This is explained by the fact that AA can promote DA oxidation and polymerization [24]. In a neutral environment, PDA is positively charged. In contrast, as the literature confirms, at neutral pH, 99.9% of AA is in the form of ascorbate (AH^-). Additionally, some studies have shown that excess AA is prone to autoxidation producing dehydroascorbic acid anions (DHA^-) [53]. The positively charged PDA will be electrostatically attracted by the ascorbate (AH^-) and dehydroascorbic acid anions (DHA^-), which will inhibit the reduction of DA on the electrode surface, leading to the formation of polydopamine. The polydopamine near the electrode surface can adsorb small molecules from the solution and thus promote the progress of DA electrochemical reactions onto the electrode surface. Other Ti-based sensors also present negligible responses for various interferences [23,25,54]. Thus, from the above results, it can be deduced that the tested electrode has good selectivity for the DA molecule, producing a clearer current response.

The feature of long-term stability was also examined, especially for cost-effective electrochemical sensors and point-of-care devices [55]. This concerns the capacity of the sensor to provide continuous and reliable monitoring of the biomolecule of interest.

The I-t curve displayed in Figure 7b represents the continuous response of the $\text{Ti}_{\text{NCs}}/\text{G}_m\text{-Cu}_{\text{foil}}$ electrode to 0.5 mM DA under a stable potential of 0.175 V, in a 0.1 M PBS electrolyte solution for 2000 s. As seen, the tested electrode exhibits long-sensing durability, after reaching its plateau current. To check repeatability and storage stability, the $\text{Ti}_{\text{NCs}}/\text{G}_m\text{-Cu}_{\text{foil}}$ electrode was conserved for 30 days at 8 °C in a 0.1 M PBS solution, and its current response for 0.5 mM DA was recorded every 6 days ($n = 6$) under the same experimental conditions (36.6 °C, pH = 7.0, 0.1 M PBS electrolyte) [56]. The resulting differential pulse voltammograms are depicted in Figure 7c. The examined electrode delivered an RSD% value of 4.8% between six different measurements, proving its ability to obtain repeatable current responses when stored in the conditions referred to above, as seen in Figure 7d. Moreover, the electrode maintained about 68% of its initial current response after 30 days of storing and periodic use, proving its storage stability. Table 2 lists analytical data for Ti-based electrodes fabricated for enzyme-free dopamine electrochemical detection, taken from similar works that appeared in international literature.

As seen in Table 2, we measured a value for the limit of detection (LOD), for 10–90 μM , higher than others reported in the literature for Ti-based electrodes. The high LOD of the as-fabricated electrode could be attributed to the Ti-nanocolumnar arrays that grew non-parallel with the atomic flux, reducing the available active sites for the reagents. The calibration curve showed two linear ranges, and the latter range had a slightly lower sensitivity. Compared to other works, $\text{Ti}_{\text{NCs}}/\text{G}_m\text{-Cu}_{\text{foil}}$ presents wider linear ranges that permit operating under considerable dopamine level variations. Moreover, the sensitivities range

in good levels. The $\text{Ti}_{\text{NCs}}/\text{G}_m\text{-Cu}_{\text{foil}}$ electrode also showed repeatability and acceptable storage stability. Its good performance toward dopamine oxidation is caused by its internal structure and active sites, while the relatively high limit of detection could be attributed to the arrays deposited on the upper parts of the substrate. For future improvements, we consider eliminating wrinkles from the substrate, which will facilitate uniform coverage and growth of Ti NCs on the graphene monolayer. This will increase the number of exposed active sites, reducing thus the LOD.

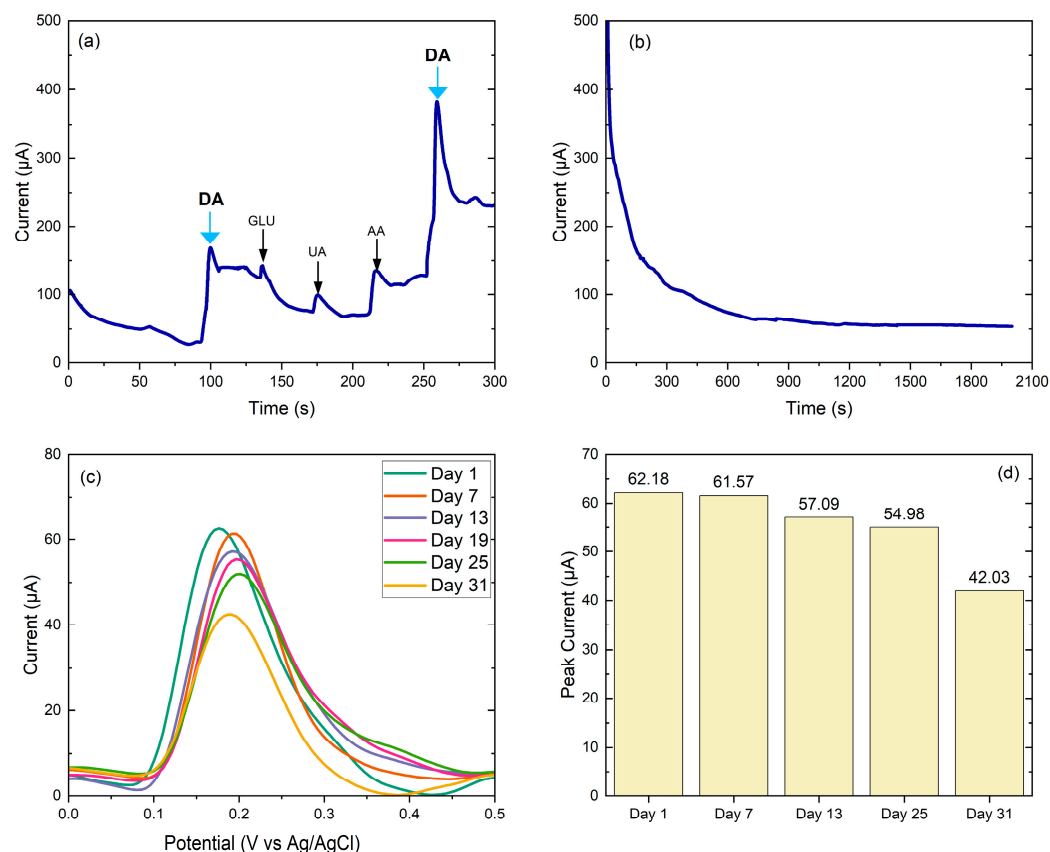


Figure 7. Amperometric response of the $\text{Ti}_{\text{NCs}}/\text{G}_m\text{-Cu}_{\text{foil}}$ electrode, conducted under the stable potential of 0.175 V with the successive addition of 1 mM of DA, Glu, UA, and AA as interfering agents (a), in the presence of 0.5 mM DA in 0.1 M PBS solution (b), DPV curves of the $\text{Ti}_{\text{NCs}}/\text{G}_m\text{-Cu}_{\text{foil}}$ electrode, recorded every 5 days, in the presence of 0.5 mM DA in 0.1 M PBS solution (c), and bar chart of DA oxidation peak current vs. the number of days, recorded every 6 days, after continuous storage of $\text{Ti}_{\text{NCs}}/\text{G}_m\text{-Cu}_{\text{foil}}$ electrode at 8 °C in 0.1 M PBS solution (d).

Table 2. Comparison of electrochemical activity between the current electrode and others reported for electrochemical detection of dopamine.

Electrode	LOD (μM)	Linear Range (μM)	Sensitivity ($\mu\text{A}\mu\text{M}^{-1}\text{cm}^{-2}$)	Refs
TiO_2/SS (stainless steel)	0.023	50.0–450.0	0.0219	[57]
C-TiN/GCE (glassy carbon electrode)	0.03	0.1–5.0 and 5.0–250.0	9.6	[23]
TiN-rGO/GCE	0.159	5.0–175.0	-	[24]
MOF- Ti_3C_2 /GCE	0.11	0.09–0.3	-	[25]
TiO_2 /GO/GCE	0.027	0.2–10.0	1.55	[54]
$\text{Ti}_{\text{NCs}}/\text{G}_m\text{-Cu}_{\text{foil}}$	6.63	10.0–90.0 and 100.0–400.0	0.14 and 0.095	This work

3. Experimental Part

3.1. Materials and Reagents

Disodium hydrogen phosphate anhydrous (Na_2HPO_4 , $\geq 99\%$), sodium dihydrogen phosphate anhydrous (NaH_2PO_4 , $>99\%$), D-glucose monohydrate (99.89%), L-ascorbic acid (99%), uric acid ($\geq 99\%$), and dopamine hydrochloride were purchased from the Sigma-Aldrich Company (Saint Louis, MO, USA). The chemicals used in this investigation were only for research and development (R&D) use and were used without further purification. Deionized water was used for all the experimental work. The 25-micron thick $\text{G}_m\text{-Cu}_{\text{foil}}$ substrate ($1 \times 1 \text{ cm}$) was bought from the CheapTubes Company (Grafton, VT, USA).

3.2. Synthesis of $\text{Ti}_{\text{NCs}}/\text{G}_m\text{-Cu}_{\text{foil}}$ Electrode

Titanium was deposited on the substrate by direct current magnetron sputtering (magnetron head model A320 from AJA Inc., Huntsville, AL, USA) in an ultra-high vacuum chamber (base pressure in the 10^{-10} mbar) using argon (Ar) as sputter gas. The Ti target has a circular shape, 2" diameter, and 0.25" thick, with 99.995% purity, and it is manufactured by AJA International (Scituate, MA, USA). An initial buffer layer of continuous Ti with 4 nm thickness was first deposited using the standard parallel configuration between the target and substrate to increase the adhesion between $\text{G}_m\text{-Cu}_{\text{foil}}$ and the metallic layer. Subsequently, the substrate tilted 75° to fabricate the nanocolumns. A deposition time of 70 min was selected to obtain nanocolumns with about 200 nm length. The distance between the circular target (5 cm diameter) and the substrate was 22 cm, the Ar pressure was 1.5×10^{-3} mbar, and the DC power was 300 W. Figure 8 provides a schematic representation of the fabrication setup [5].

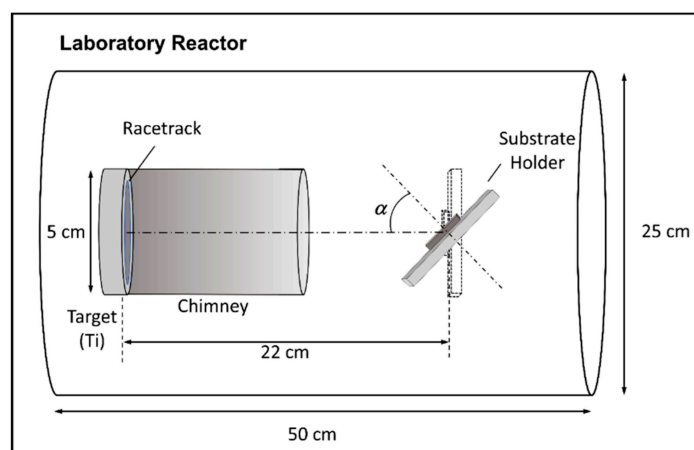


Figure 8. Schematic representation of the laboratory reactor employed to grow the Ti nanocolumns [5], reproduced under the CC BY 4.0 license.

3.3. Structural Characterization

The $\text{Ti}_{\text{NCs}}/\text{G}_m\text{-Cu}_{\text{foil}}$ electrode microstructure was analyzed by scanning electron microscopy (SEM, Hong Kong, FEI Verios 460). The surface morphology was examined by recording atomic force microscopy (AFM, Bruker Dimension Icon, Billerica, MA, USA) images in non-contact mode using commercial probes (model NT-TP-HRES from NEXT-TIP, Seattle, WA, USA) with 330 kHz resonance frequency, 40 N spring constant, and a 2 nm nominal radius. The elemental composition of the film was studied by the same scanning electron microscope attached with an energy dispersive analysis of an X-ray (EDAX, Pleasanton, CA, USA) analyzer.

3.4. Electrochemical Characterizations

The electrocatalytic behavior of the as-fabricated electrode was tested with cyclic voltammetry (CV), differential pulse voltammetry (DPV), and chronoamperometry (CA)

electrochemical techniques. The electrochemical measurements were performed with the aid of the PalmSens4 potentiostat/galvanostat in a conventional 3-electrode electrochemical cell (AMEL, Chem.), using Ag/AgCl (3 M KCl) as the reference electrode (RE) and a graphite rod as the counter electrode (CE).

All voltages are relative to Ag/AgCl. All the electrochemical measurements were conducted in a 0.1 M phosphate buffer solution (PBS) of pH = 7.0, while the temperature was held at 36.6 °C with the aid of a recirculating thermostat (Wise Circu-Wisd, TechnoLab, T'bilisi, GA, USA). For the estimation of the PBS pH, the Henderson-Hasselbalch equation (Equation (3)) [58] was used:

$$\text{pH} = \text{pK}_a + \log \left(\frac{[\text{A}^-]}{[\text{HA}]} \right) \quad (3)$$

where $[\text{A}^-]$ and $[\text{HA}]$ refer to the base and acid concentrations. Before each measurement, the solution was purged with N_2 gas to create an inert atmosphere, and the working electrode was electrochemically conditioned from -0.70 to 1.10 V with a scan rate of 100 mV/s until stable cycles were achieved. CV measurements were conducted from -0.70 to 1.10 V. DPV experiments were recorded from 0.0 to 0.50 V, with step potential 2.0 mV, pulse potential 0.20 V, and pulse time 0.3 s. CA was conducted at a stable potential of 0.175 V, close to the DA oxidation potential.

4. Conclusions

In the present work, a PVD method by magnetron sputtering at oblique angle (75°) was adopted, and the fabrication of a thin film of Ti-nanocolumnar arrays of 200 nm average height was achieved. Over the as-fabricated electrode, dopamine electrooxidation reaction is facilitated, allowing the quasi-reversible electrooxidation of protonated dopamine to dopamine quinone, and contrary to many works reported in the literature, also favors further quasi-reversible oxidation of leucodopaminechrome to dopaminechrome. This performance is attributed to the development of a greatly efficient interface permitted by Ti nanostructure special morphology arrangement. Moreover, the $\text{Ti}_{\text{NCs}}/\text{G}_m\text{-Cu}_{\text{foil}}$ electrode presented two linear ranges of dopamine detection that permit operating under considerable dopamine level variation with great stability. However, the selectivity of the electrode should be further ameliorated.

Supplementary Materials: The following supporting information can be downloaded at: <https://www.mdpi.com/article/10.3390/catal14080478/s1>. Figure S1. Optical image of the substrate. The red cycle indicates the flat areas (a), AFM images of the substrate (b), photos of the substrate before (c) and after deposition (d).

Author Contributions: Conceptualization, G.B., A.B. and P.T.; methodology, G.B., E.G. and A.B.; validation, C.L.V., V.B., A.B. and P.T.; formal analysis, G.B., J.M.G.-M., E.G. and A.B.; investigation, G.B., J.M.G.-M., E.G. and A.B.; writing—original draft preparation, G.B., J.M.G.-M. and A.B.; supervision, A.B. and P.T. All authors have read and agreed to the published version of the manuscript.

Funding: This research was funded by the [Hellenic Foundation for Research and Innovation] [Fellowship Number: 05869] (G.B.); the [Ministry of Science and Innovation, Spain] [grant PID2021-126524NB-I00] (J.M.G.-M) and the [University of Thessaly] [5600.03.08.05] (A.B.).

Data Availability Statement: Data are contained within the article and Supplementary Files.

Acknowledgments: G.B. is grateful to the Hellenic Foundation for Research and Innovation (H.F.R.I.) under the “3rd Call for H.F.R.I. Ph.D. Fellowships” (Fellowship Number: 05869) for funding; J.M.G.-M. thanks grant PID2021-126524NB-I00 funded by MCIN/AEI/ 10.13039/501100011033 and by “ERDF A way of making Europe”; A.B. thankfully acknowledges the Research, Innovation, and Excellence Structure (DEKA) of the University of Thessaly for funding (5600.03.08.05).

Conflicts of Interest: The authors declare no conflicts of interest.

References

1. Channer, B.; Matt, S.M.; Nickoloff-Bybel, E.A.; Pappa, V.; Agarwal, Y.; Wickman, J.; Gaskill, P.J. Dopamine, Immunity, and Disease. *Pharmacol. Rev.* **2023**, *75*, 62–158. [[CrossRef](#)] [[PubMed](#)]
2. Vayenas, C.G.; Bebelis, S.; Yentekakis, I.V.; Tsiakaras, P.; Karasali, H. Non-Faradaic Electrochemical Modification of Catalytic Activity. *Platin. Met. Rev.* **1990**, *34*, 122–130. [[CrossRef](#)]
3. Liu, D.; Barbar, A.; Najam, T.; Javed, M.S.; Shen, J.; Tsiakaras, P.; Cai, X. Single noble metal atoms doped 2D materials for catalysis. *Appl. Catal. B Environ.* **2021**, *297*, 120389. [[CrossRef](#)]
4. Volkov, A.; Gorbova, E.; Vylkov, A.; Medvedev, D.; Demin, A.; Tsiakaras, P. Design and applications of potentiometric sensors based on proton-conducting ceramic materials. A brief review. *Sens. Actuators B Chem.* **2017**, *244*, 1004–1015. [[CrossRef](#)]
5. Gorbova, E.; Balkourani, G.; Molochas, C.; Sidiropoulos, D.; Brouzgou, A.; Demin, A.; Tsiakaras, P. Brief Review on High-Temperature Electrochemical Hydrogen Sensors. *Catalysts* **2022**, *12*, 1647. [[CrossRef](#)]
6. Kalyakin, A.; Demin, A.K.; Gorbova, E.; Volkov, A.; Tsiakaras, P.E. Sensor Based on a Solid Oxide Electrolyte for Measuring the Water-Vapor and Hydrogen Content in Air. *Catalysts* **2022**, *12*, 1558. [[CrossRef](#)]
7. Brouzgou, A.; Tsiakaras, P. Electrocatalysts for Glucose Electrooxidation Reaction: A Review. *Top. Catal.* **2015**, *58*, 1311–1327. [[CrossRef](#)]
8. Brouzgou, A.; Gorbova, E.; Wang, Y.; Jing, S.; Seretis, A.; Liang, Z.; Tsiakaras, P. Nitrogen-doped 3D hierarchical ordered mesoporous carbon supported palladium electrocatalyst for the simultaneous detection of ascorbic acid, dopamine, and glucose. *Ionics* **2019**, *25*, 6061–6070. [[CrossRef](#)]
9. Brouzgou, A.; Lo Vecchio, C.; Baglio, V.; Aricò, A.S.; Liang, Z.X.; Demin, A.; Tsiakaras, P. Glucose electrooxidation reaction in presence of dopamine and uric acid over ketjenblack carbon supported PdCo electrocatalyst. *J. Electroanal. Chem.* **2019**, *855*, 113610. [[CrossRef](#)]
10. Alvarez, R.; Muñoz-Piña, S.; González, M.U.; Izquierdo-Barba, I.; Fernández-Martínez, I.; Rico, V.; Arcos, D.; García-Valenzuela, A.; Palmero, A.; Vallet-Regi, M. Antibacterial nanostructured Ti coatings by magnetron sputtering: From laboratory scales to industrial reactors. *Nanomaterials* **2019**, *9*, 1217. [[CrossRef](#)]
11. Sajjan, V.A.; Mohammed, I.; Nemakal, M.; Aralekallu, S.; Hemantha Kumar, K.R.; Swamy, S.; Sannegowda, L.K. Synthesis and electropolymerization of cobalt tetraaminebenzamidephthalocyanine macrocycle for the amperometric sensing of dopamine. *J. Electroanal. Chem.* **2019**, *838*, 33–40. [[CrossRef](#)]
12. Brouzgou, A. Graphene-based Nanomaterials as Organocatalyst. In *Graphene-Based Nanomaterial Catalysis*; Singh, M., Rai, V.K., Rai, A., Eds.; Bentham Science Publishers Pte.: Singapore, 2022; Chapter 2; pp. 24–42.
13. Melníková-Komínková, Z.; Valeš, V.; Frank, O.; Kalbáč, M. Evolution of the Raman 2D' mode in monolayer graphene during electrochemical doping. *Microchem. J.* **2022**, *181*, 107739. [[CrossRef](#)]
14. Zhang, Y.Y.; Gu, Y.T. Mechanical properties of graphene: Effects of layer number, temperature and isotope. *Comput. Mater. Sci.* **2013**, *71*, 197–200. [[CrossRef](#)]
15. Song, H.; Zhang, X.; Liu, Y.; Su, Z. Developing Graphene-Based Nanohybrids for Electrochemical Sensing. *Chem. Rec.* **2019**, *19*, 534–549. [[CrossRef](#)] [[PubMed](#)]
16. Xu, S.; Zhang, L.; Wang, B.; Ruoff, R.S. Chemical vapor deposition of graphene on thin-metal films. *Cell Rep. Phys. Sci.* **2021**, *2*, 100372. [[CrossRef](#)]
17. Kuntoji, G.; Kousar, N.; Gaddimath, S.; Koodlur Sannegowda, L. Macromolecule–Nanoparticle-Based Hybrid Materials for Biosensor Applications. *Biosensors* **2024**, *14*, 277. [[CrossRef](#)]
18. Khoshroo, A.; Sadrjavadi, K.; Taran, M.; Fattahi, A. Electrochemical system designed on a copper tape platform as a nonenzymatic glucose sensor. *Sens. Actuators B Chem.* **2020**, *325*, 128778. [[CrossRef](#)]
19. Chen, L.-Y.; Cui, Y.-W.; Zhang, L.-C. Recent development in beta titanium alloys for biomedical applications. *Metals* **2020**, *10*, 1139. [[CrossRef](#)]
20. Sarraf, M.; Rezvani Ghomi, E.; Alipour, S.; Ramakrishna, S.; Liana Sukiman, N. A state-of-the-art review of the fabrication and characteristics of titanium and its alloys for biomedical applications. *Bio-Des. Manuf.* **2022**, *5*, 371–395. [[CrossRef](#)]
21. Bertel, L.; Miranda, D.A.; García-Martín, J.M. Nanostructured titanium dioxide surfaces for electrochemical biosensing. *Sensors* **2021**, *21*, 6167. [[CrossRef](#)]
22. Pandey, L.M. Design of biocompatible and self-antibacterial titanium surfaces for biomedical applications. *Curr. Opin. Biomed. Eng.* **2023**, *25*, 100423. [[CrossRef](#)]
23. Wang, C.; Li, W.; Long, Y. Molten salt-assisted synthesis of C-TiN nanocomposites for sensitive dopamine determination. *Mater. Lett.* **2022**, *329*, 133234. [[CrossRef](#)]
24. Feng, J.; Li, Q.; Cai, J.; Yang, T.; Chen, J.; Hou, X. Electrochemical detection mechanism of dopamine and uric acid on titanium nitride-reduced graphene oxide composite with and without ascorbic acid. *Sens. Actuators B Chem.* **2019**, *298*, 126872. [[CrossRef](#)]
25. Paul, J.; Kim, J. Reticular synthesis of a conductive composite derived from metal-organic framework and Mxene for the electrochemical detection of dopamine. *Appl. Surf. Sci.* **2023**, *613*, 156103. [[CrossRef](#)]
26. Kulkarni, M.; Mazare, A.; Gongadze, E.; Perutkova, Š.; Kralj-Iglič, V.; Milošev, I.; Schmuki, P.; Iglič, A.; Mozetič, M. Titanium nanostructures for biomedical applications. *Nanotechnology* **2015**, *26*, 062002. [[CrossRef](#)] [[PubMed](#)]
27. Levin, M.; Spiro, R.C.; Jain, H.; Falk, M.M. Effects of titanium implant surface topology on bone cell attachment and proliferation in vitro. *Med. Devices Evid. Res.* **2022**, *15*, 103–119. [[CrossRef](#)]

28. Zhang, J.; Siddiqui, M.K.; Rauf, A.; Ishtiaq, M. On ve-degree and ev-degree based topological properties of single walled titanium dioxide nanotube. *J. Clust. Sci.* **2021**, *32*, 821–832. [CrossRef]
29. Alvarez, R.; Garcia-Martin, J.M.; Garcia-Valenzuela, A.; Macias-Montero, M.; Ferrer, F.J.; Santiso, J.; Rico, V.; Cotrino, J.; Gonzalez-Elipe, A.R.; Palmero, A. Nanostructured Ti thin films by magnetron sputtering at oblique angles. *J. Phys. D Appl. Phys.* **2016**, *49*, 045303. [CrossRef]
30. Mobini, S.; González, M.U.; Caballero-Calero, O.; Patrick, E.E.; Martín-González, M.; García-Martín, J.M. Effects of nanostructuration on the electrochemical performance of metallic bioelectrodes. *Nanoscale* **2022**, *14*, 3179–3190. [CrossRef]
31. Rocha, J.F.; Hasimoto, L.H.; Santhiago, M. Recent progress and future perspectives of polydopamine nanofilms toward functional electrochemical sensors. *Anal. Bioanal. Chem.* **2023**, *415*, 3799–3816. [CrossRef]
32. Izquierdo-Barba, I.; García-Martín, J.M.; Álvarez, R.; Palmero, A.; Esteban, J.; Pérez-Jorge, C.; Arcos, D.; Vallet-Regí, M. Nanocolumnar coatings with selective behavior towards osteoblast and Staphylococcus aureus proliferation. *Acta Biomater.* **2015**, *15*, 20–28. [CrossRef]
33. Peláez-Abellán, E.; Rocha-Sousa, L.; Müller, W.-D.; Guastaldi, A.C. Electrochemical stability of anodic titanium oxide films grown at potentials higher than 3 V in a simulated physiological solution. *Corros. Sci.* **2007**, *49*, 1645–1655. [CrossRef]
34. Azumi, K.; Seo, M. Changes in electrochemical properties of the anodic oxide film formed on titanium during potential sweep. *Corros. Sci.* **2001**, *43*, 533–546. [CrossRef]
35. Muguruma, H.; Inoue, Y.; Inoue, H.; Ohsawa, T. Electrochemical study of dopamine at electrode fabricated by cellulose-assisted aqueous dispersion of long-length carbon nanotube. *J. Phys. Chem. C* **2016**, *120*, 12284–12292. [CrossRef]
36. Biswas, B.; Singh, P.C. Protonation State of Dopamine Neurotransmitter at the Aqueous Interface: Vibrational Sum Frequency Generation Spectroscopy Study. *Langmuir* **2022**, *38*, 1380–1385. [CrossRef]
37. Yang, Y.; Li, M.; Zhu, Z. A novel electrochemical sensor based on carbon nanotubes array for selective detection of dopamine or uric acid. *Talanta* **2019**, *201*, 295–300. [CrossRef]
38. Balkourani, G.; Brouzgou, A.; Tsiakaras, P. A review on recent advancements in electrochemical detection of dopamine using carbonaceous nanomaterials. *Carbon* **2023**, *213*, 118281. [CrossRef]
39. Schindler, S.; Bechtold, T. Mechanistic insights into the electrochemical oxidation of dopamine by cyclic voltammetry. *J. Electroanal. Chem.* **2019**, *836*, 94–101. [CrossRef]
40. Jacobs, C.B.; Ivanov, I.N.; Nguyen, M.D.; Zestos, A.G.; Venton, B.J. High temporal resolution measurements of dopamine with carbon nanotube yarn microelectrodes. *Anal. Chem.* **2014**, *86*, 5721–5727. [CrossRef] [PubMed]
41. Nazari, Z.; Hadi Nematollahi, M.; Zareh, F.; Pouramiri, B.; Mehrabani, M. An electrochemical sensor based on carbon quantum dots and ionic liquids for selective detection of dopamine. *ChemistrySelect* **2023**, *8*, e202203630. [CrossRef]
42. Selvolini, G.; Lazzarini, C.; Marrazza, G. Electrochemical nanocomposite single-use sensor for dopamine detection. *Sensors* **2019**, *19*, 3097. [CrossRef] [PubMed]
43. Neupane, M.P.; Park, I.S.; Lee, S.J.; Kim, K.A.; Lee, M.H.; Bae, T.S. Study of Anodic Oxide Films of Titanium Fabricated by Voltammetric Technique in Phosphate Buffer Media. *Int. J. Electrochem. Sci.* **2009**, *4*, 197–207. [CrossRef]
44. Wan, M.; Jimu, A.; Yang, H.; Zhou, J.; Dai, X.; Zheng, Y.; Ou, J.; Yang, Y.; Liu, J.; Wang, L. MXene quantum dots enhanced 3D-printed electrochemical sensor for the highly sensitive detection of dopamine. *Microchem. J.* **2023**, *184*, 108180. [CrossRef]
45. Sriram, B.; Kogularasu, S.; Wang, S.-F.; Sheu, J.-K. Deep eutectic solvent-mediated synthesis of spinel zinc chromite nanoparticles: A simple label-free electrochemical sensor for dopamine and ascorbic acid. *ACS Appl. Nano Mater.* **2023**, *6*, 17593–17602. [CrossRef]
46. Ahmed, J.; Faisal, M.; Alsareii, S.; Jalalah, M.; Harraz, F.A. A novel gold-decorated porous silicon-poly (3-hexylthiophene) ternary nanocomposite as a highly sensitive and selective non-enzymatic dopamine electrochemical sensor. *J. Alloys Compd.* **2023**, *931*, 167403. [CrossRef]
47. Niu, B.; Liu, M.; Li, X.; Guo, H.; Chen, Z. Vein-like Ni-BTC@ Ni₃S₄ with sulfur vacancy and Ni³⁺ fabricated in situ etching vulcanization strategy for an electrochemical sensor of dopamine. *ACS Appl. Mater. Interfaces* **2023**, *15*, 13319–13331. [CrossRef]
48. Zhang, L.; Tang, J.; Li, J.; Li, Y.; Yang, P.; Zhao, P.; Fei, J.; Xie, Y. A novel dopamine electrochemical sensor based on 3D flake nickel oxide/cobalt oxide@ porous carbon nanosheets/carbon nanotubes/electrochemical reduced of graphene oxide composites modified glassy carbon electrode. *Colloids Surf. A Physicochem. Eng. Asp.* **2023**, *666*, 131284. [CrossRef]
49. Saha, S.; Sarkar, P.; Turner, A.P.F. Interference-Free Electrochemical Detection of Nanomolar Dopamine Using Doped Polypyrrole and Silver Nanoparticles. *Electroanalysis* **2014**, *26*, 2197–2206. [CrossRef]
50. Golrokh Amin, B.; De Silva, U.; Masud, J.; Nath, M. Ultrasensitive and Highly Selective Ni₃Te₂ as a Nonenzymatic Glucose Sensor at Extremely Low Working Potential. *ACS Omega* **2019**, *4*, 11152–11162. [CrossRef] [PubMed]
51. European Medicines Agency, S.M.H., ICH Q2(R2) Guideline on Validation of Analytical Procedures. 2023. Available online: https://www.ema.europa.eu/en/documents/scientific-guideline/ich-q2r2-guideline-validation-analytical-procedures-step-5-revision-1_en.pdf (accessed on 30 June 2024).
52. Zhao, D.; Yu, G.; Tian, K.; Xu, C. A highly sensitive and stable electrochemical sensor for simultaneous detection towards ascorbic acid, dopamine, and uric acid based on the hierarchical nanoporous PtTi alloy. *Biosens. Bioelectron.* **2016**, *82*, 119–126. [CrossRef]
53. Zou, M.-Y.; Nie, S.-P.; Yin, J.-Y.; Xie, M.-Y. Ascorbic acid induced degradation of polysaccharide from natural products: A review. *Int. J. Biol. Macromol.* **2020**, *151*, 483–491. [CrossRef] [PubMed]
54. Josephine, D.S.R.; Babu, K.J.; Gnana Kumar, G.P.; Sethuraman, K. Titanium dioxide anchored graphene oxide nanosheets for highly selective voltammetric sensing of dopamine. *Microchim. Acta* **2017**, *184*, 781–790. [CrossRef]

55. Babaei, A.; Taheri, A.R. Nafion/Ni(OH)₂ nanoparticles-carbon nanotube composite modified glassy carbon electrode as a sensor for simultaneous determination of dopamine and serotonin in the presence of ascorbic acid. *Sens. Actuators B Chem.* **2013**, *176*, 543–551. [[CrossRef](#)]
56. Mani, V.; Govindasamy, M.; Chen, S.-M.; Karthik, R.; Huang, S.-T. Determination of dopamine using a glassy carbon electrode modified with a graphene and carbon nanotube hybrid decorated with molybdenum disulfide flowers. *Microchim. Acta* **2016**, *183*, 2267–2275. [[CrossRef](#)]
57. Amir, H.; Ponpandian, N.; Viswanathan, C. An electrochemical dopamine sensor based on RF magnetron sputtered TiO₂/SS thin film electrode. *Mater. Lett.* **2021**, *300*, 130175. [[CrossRef](#)]
58. Po, H.N.; Senozan, N.M. The Henderson-Hasselbalch Equation: Its History and Limitations. *J. Chem. Educ.* **2001**, *78*, 1499. [[CrossRef](#)]

Disclaimer/Publisher’s Note: The statements, opinions and data contained in all publications are solely those of the individual author(s) and contributor(s) and not of MDPI and/or the editor(s). MDPI and/or the editor(s) disclaim responsibility for any injury to people or property resulting from any ideas, methods, instructions or products referred to in the content.